







Distribution of Europium in The Milky Way Disk; Its Connection to Planetary Habitability and The Source of The R-Process

EVAN M. CARRASCO ¹, MATTHEW SHETRONE ², FRANCIS NIMMO ³, ENRICO RAMIREZ-RUIZ ¹, JOEL PRIMACK ⁴,
AND NATALIE M. BATALHA ¹

¹*Department of Astronomy and Astrophysics, University of California, Santa Cruz, CA 95064, USA*

²*University of California Observatories, CA 95064, USA*

³*Department of Earth and Planetary Sciences, University of California, Santa Cruz, CA 95064, USA*

⁴*Physics Department, University of California Santa Cruz, 1156 High Street, Santa Cruz, CA 95064 USA*

ABSTRACT

The energy provided in the radioactive decay of thorium (Th) and uranium (U) isotopes, embedded in planetary mantles, sustains geodynamics important for surface habitability such as the generation of a planetary magnetic dynamo. In order to better understand the thermal evolution of nearby exoplanets, stellar photospheric abundances can be used to infer the material composition of orbiting planets. Here we constrain the intrinsic dispersion of the r-process element europium (Eu) (measured in relative abundance [Eu/H]) as a proxy for Th and U in local F, G, and K type dwarf stars. Adopting stellar-chemical data from two high quality spectroscopic surveys, we have determined a small intrinsic scatter of 0.025 dex in [Eu/H] within the disk. We further investigate the stellar anti-correlation in [Eu/ α] vs [α /H] at late metallicities to probe in what regimes planetary radiogenic heating may lead to periods of extended dynamo collapse. We find that only near-solar metallicity stars in the disk have Eu inventories supportive of a persistent dynamo in attendant planets, supporting the notion of a “metallicity Goldilocks zone” in the galactic disk. The observed anti-correlation further provides novel evidence regarding the nature of r-processes injection by substantiating α element production is decoupled from Eu injection. This suggests either a metallicity-dependent r-process in massive core-collapse supernovae, or that neutron-star merger events dominate r-process production in the recent universe.

Keywords: Exoplanet evolution; Astrobiology; Magnetic fields; R-process; Stellar nucleosynthesis

1. INTRODUCTION

Geological activity on rocky planets is driven by various thermal inputs from formational and long-lived heat sources. The majority of a planet’s thermal inventory is provided in the first few Myr during planetary accretion, which sets the initial conditions for a planet’s evolution. Long-term heating sources such as tidal forces and radiogenic heating act on extended time scales and come to dominate the thermal dynamics of mature planets. Tidal heating is largely dependent on the geometry of a given planetary system and can be difficult to constrain. Whereas radiogenic heating, the focus of the study herein, operates in a robust manner on time scales of Gyrs, shaping planetary evolution across a broad population of terrestrial planets.

Long-lived radioisotopes thorium-232 (²³²Th), uranium-235 (²³⁵U), and uranium-238 (²³⁸U) are em-

bedded in the mantle/crusts of rocky planets.¹ Over geological times scales (Gyrs) they undergo decay, releasing energy into the mantle.

Radiogenic heating impacts a wide variety of planetary processes important to surface conditions; Frank et al. (2014); Jellinek & Jackson (2015); Botelho et al. (2019); Unterborn et al. (2015); Foley & Smye (2018); Quick et al. (2020); Zhang & Rogers (2022); Boujibar et al. (2020); Wang et al. (2020); Mello & Friaça (2023). Here we focus on the generation of a magnetic field and its effect on atmospheric preservation. A magnetic dynamo is driven by convection in a rotating planet’s liquid core, the strength of which is moderated by the thermal

¹ Potassium-40 (⁴⁰K) is another significant contributor included in our modeling; however, because of its relatively short half-life of 1.25 Gyr its contribution is modest at late times (see also Nimmo et al. 2020).

exchange across the core-mantle boundary (Labrosse 2014). This rate of exchange, and by extension the vigor of the dynamo, is strongly dependent upon radiogenic heating. Excessive mantle heating caused by an over-abundance of radioactive elements reduces the heat extracted from the core and thus the thermal buoyancy available to drive core convection. This leads to a period of dynamo-failure² (Nimmo et al. 2020; Labrosse 2015; Boujibar et al. 2020). A robust magnetic dynamo is considered a defining feature of Earth’s habitable biosphere, protecting the surface from intense solar irradiation, preserving the atmosphere and liquid water inventories. On Earth, the geodynamo has persisted for at least the last 3.7 Gyr with no interruptions (e.g., Nichols et al. 2024), although the magnetic field has occasionally dropped to as low as one-tenth of its mean value (Bono et al. 2019).

Relevant to this study are the works by O’Neill et al. (2020) and Nimmo et al. (2020), wherein variations of Th and U concentrations in Earth-like exoplanet mantles affect the generation of a persistent magnetic dynamo. O’Neill et al. (2020) assume variations of Th and U are small between planets and correlated with core size. While Nimmo et al. (2020) assume larger systematic variation in Th and U, motivated by the observed scatter at early times of the proxy element Eu in dwarf galaxies (Ji et al. 2016) and low-metallicity stars (Arnould et al. 2007; Sneden et al. 2008; Macias & Ramirez-Ruiz 2018; Kolborg et al. 2023). In Section 4, we adopt the model described in Nimmo et al. (2020) to predict at what radioactive element content we expect a persistent dynamo failure based on the real distribution of elements in the disk.

The planetary abundances of refractory elements (such as the isotopes of interest) should reflect the abundances of the host star, given that planet and host star form from a common natal molecular cloud (e.g., Naiman et al. 2018). While lighter elements have complicated radial dependencies due to ice lines, here we assume metals and radioactive elements are distributed homogeneously between star and rocky planet.

Th and U nuclei are formed almost exclusively by the rapid neutron-capture process (r-process) in rare, cataclysmic events such as neutron star-neutron star mergers (NS-NS mergers; Kasen et al. 2017) and/or extreme flavors of core collapse supernovae (CC-SNe; Cowan & Thielemann 2004; Mösta et al. 2018; Siegel et al. 2019), although the dominant production mechanism is still of debate (Cescutti et al. 2005; Macias & Ramirez-Ruiz

2019; Holmbeck et al. 2023). The relative abundance³ of [Th/H] and [U/H] can be difficult to measure in stellar spectra due to line blending. Instead, the r-process element europium (Eu) is commonly used as a proxy element as it follows the same nucleosynthetic channels but has reasonably strong and distinct absorption features in stellar spectra. [Eu/H] tracks well with [U/H] (Sneden et al. 2008) and [Th/H] (Botelho et al. 2019) in the galactic disk. Existing literature suggests a wide star-to-star scatter of Eu at low metallicities and in halo stars (e.g., Sneden et al. 2008; Kolborg et al. 2023). Here we focus on constraining the variation of Eu as a proxy for Th and U at planet-forming metallicities, estimated to be between -1.5 and +0.6 [Fe/H] in the Milky Way (MW) disk (e.g., Johnson & Li 2012; Ercolano & Clarke 2010; Behroozi & Peeples 2015; Boley et al. 2024) to place meaningful constraints on the thermal evolution of attendant Earth-like planets.

2. METHODOLOGY

The Eu abundance analysis in our study is based on two independent surveys in the literature: 1) a survey of 1111 F,G, and K type stars observed as a part of the HARPS GTO planet search program (Delgado Mena et al. 2017) (hereafter referred to as DM) and 2) a multi-telescope campaign to observe 714 F and G type stars in the solar neighborhood Battistini & Bensby (2016) and Bensby et al. (2014) (hereafter referred to as BB). Both samples represent extremely high S/N surveys of the local stellar F,G, and K population. The sample from DM contains 577 stars with usable Eu measurements using the red 6645 Å absorption line. The sample from BB contains 377 stars with usable Eu measurements using the blue 4129 Å absorption line.

Initially, the dispersion of [Eu/H] in both samples appears large, but we show this is the result of systematic inflation due to a metallicity ([α /H]) and effective-temperature (T_{eff}) dependence on [Eu/H] abundance. To mitigate these biases and recover the true star-to-star dispersion in [Eu/H], we detrend both samples using a linear contour (plane) fit to each sample.

2.1. Systematic Biases in Metallicity - α Elements

The metallicity dependence is representative of an astrophysical bias consequence of stellar evolution. Colloquially, metallicity refers to [Fe/H], a well established stellar evolutionary probe. However, in this study we have elected to use an α element based metallicity:

² A similar effect may occur at Io, driven by excessive tidal heating in the mantle (Wienbruch & Spohn 1995).

³ Here we adopt the standard notation where the relative abundance of elements A and B in a given star compared to the sun can be written as $[A/B] = \log_{10}(N_A/N_B)_\star - \log_{10}(N_A/N_B)_\odot$.

$[\alpha/\text{H}]$. This is motivated by chemical differentiation within the stellar neighborhood in the high- α and low- α groups (correlated with the thick and thin disk of the MW). High- α population stars have systematically larger $[\text{Eu}/\text{H}]$ abundances than the low- α population stars, making the correlation between $[\text{Fe}/\text{H}]$ and $[\text{Eu}/\text{H}]$ distinct for each group. Instead of conducting analysis on each population separately we fit metallicity as $[\alpha/\text{H}]$. $[\text{Fe}/\text{H}]$ and $[\alpha/\text{H}]$ are both well connected to stellar evolution; however, in this context $[\alpha/\text{H}]$ serves the distinct advantage of coupling metallicity to the galactic α population while still being a robust probe for stellar evolution.

Our α metallicity term is defined as the average of silicon (Si), magnesium (Mg), titanium (Ti), and calcium (Ca). Si and Mg are the typical elements used to describe α element abundance, while Ti and Ca are incorporated to reduce the measurement uncertainty through averaging of all four elements which track each other closely in the stellar neighborhood.

2.2. Systematic Biases in T_{eff}

The bias in effective temperature (T_{eff}) is not reflective of any astrophysical process; in principle T_{eff} should not chemically have an effect on $[\text{Eu}/\text{H}]$ abundance. However, we find in the sample from DM that cool stars have systematically lower $[\text{Eu}/\text{H}]$ than hot stars, while in the sample from BB there is an anti-correlation between T_{eff} and $[\text{Eu}/\text{H}]$. This bias is likely representative of a methodological bias introduced in elemental parameters for abundance measurement in each study.

2.3. Detrended Contour Fitting

The identified biases inflate the star-to-star dispersion in $[\text{Eu}/\text{H}]$ and are removed via regression of a linear contour fit simultaneously to $[\alpha/\text{H}]$ and T_{eff} . This is done using the IRAF task *Surfit*, under a reduced χ -squared test. The best fit coefficients are shown in Table 1.

An expression for detrended $[\text{Eu}/\text{H}]$ as a function of metallicity and temperature is created by subtracting the contour fit from $[\text{Eu}/\text{H}]$ for each sample, this function represents the $[\text{Eu}/\text{H}]$ independent of metallicity and T_{eff} . The standard deviation about detrended $[\text{Eu}/\text{H}]$, is 0.071 dex and 0.081 dex in samples by DM, and BB, respectively.

3. RESULTS AND ANALYSIS

3.1. Combining Data Sets

While the two samples from DM, and BB represent some of the highest quality chemical measurements available on the stellar neighborhood, there are still inconsistencies in measured $[\text{Eu}/\text{H}]$ between stars in each

sample. In an attempt to reduce these inconsistencies, we create a cross-matched sample of the 68 stars that appear in common between these surveys and average their detrended $[\text{Eu}/\text{H}]$ expressions. Under the cross matched sample the standard deviation about detrended $[\text{Eu}/\text{H}]$ is reduced to 0.057 dex and 0.065 dex for DM, and BB, respectively.

3.2. Intrinsic Dispersion

Cross matching our samples provides an opportunity to reduce the uncertainty associated with detrended $[\text{Eu}/\text{H}]$ even further. If the detrended $[\text{Eu}/\text{H}]$ dispersion is contributed entirely by Poisson noise, we would expect the dispersion about the averaged detrended $[\text{Eu}/\text{H}]$ to reduce by a factor of $1/\sqrt{2}$. However we find this is not the case; The average detrended $[\text{Eu}/\text{H}]$ scatter is only 0.047 dex. This would imply there is a secondary factor dominating the detrended $[\text{Eu}/\text{H}]$ spread. We refer to this term as the *intrinsic dispersion*, which can be solved for:

To begin, the total error budget is assumed to be the sum of three terms: uncertainty contributed by Poisson noise, uncertainty contributed by systematic biases in the data, and the independent intrinsic term. Thus the error budget on detrended $[\text{Eu}/\text{H}]$ for both sample from DM and BB can be written as Equation 1:

$$\sigma_{\text{Total}}^2 = \sigma_{\text{Poisson}}^2 + \sigma_{\text{Systematic}}^2 + \sigma_{\text{Intrinsic}}^2 \quad (1)$$

In the creation of the detrended $[\text{Eu}/\text{H}]$ expression, all significant systematic biases (metallicity and temperature) have been removed. Therefore we assume the uncertainty contributed by symmetric biases is effectively removed. The total error budget is then written as the sum of only the Poisson and intrinsic terms. When combining data samples, the resulting uncertainty associated with the average detrended $[\text{Eu}/\text{H}]$ can be represented as the average of the two total error budgets from each sample. The intrinsic term should be constant across both samples and thus can be combined.

$$\sigma_{\text{Average}}^2 = \frac{\sigma_{\text{PoissonDM}}^2 + \sigma_{\text{PoissonBB}}^2 + 2\sigma_{\text{Intrinsic}}^2}{4} \quad (2)$$

Which is then rearranged to solve for the constant intrinsic uncertainty in equation 3:

$$\sigma_{\text{Intrinsic}} = \sqrt{2\sigma_{\text{Average}}^2 - \frac{\sigma_{\text{PoissonDM}}^2 + \sigma_{\text{PoissonBB}}^2}{2}} \quad (3)$$

This results in an intrinsic uncertainty of $\sigma_{\text{Intrinsic}} = 0.025$ dex. We believe this to be the intrinsic star-to-star variation in $[\text{Eu}/\text{H}]$ in the stellar neighborhood of F, G and K type stars in the MW disk independent

Sample	Zero-point	$[\alpha/H]$ Slope	T_{eff} Slope
Delgado Mena et al. (2017)	0.521 ± 0.055	0.844 ± 0.016	$-9.14 \times 10^{-5} \pm 9.669 \times 10^{-6}$
Bensby et al. (2014) and Battistini & Bensby (2016)	-0.527 ± 0.099	0.768 ± 0.022	$9.78 \times 10^{-5} \pm 1.71 \times 10^{-5}$

Table 1. Second order fitting polynomials for the DM and BB samples, fit to temperature (T_{eff}) and metallicity ($[\alpha/H]$). A function of detrended $[\text{Eu}/H]$ is created by subtracting the above expressions from $[\text{Eu}/H]$ for each sample. The cross-matched expression is given as an average of the DM and BB expressions.

of metallicity and temperature biases. The identified dispersion is corroborated by the solar twins analysis by Bedell et al. (2018) and Spina et al. (2018) discussed in Section 7.1. outliers in the samples are discussed in Appendix 7.2.

4. DISCUSSION

4.1. Implications on Dynamo Shutoff Range

Decay of radioactive elements in the mantles of rocky planets moderates geodynamic processes, such as a protective planetary magnetic dynamo - an excessive amount of radioactive heating can disrupt core convection responsible for maintaining a magnetic dynamo (Nimmo et al. 2020). While the effect of magnetic dynamo failure on atmospheric loss is still debated (e.g., Gunell et al. 2018), it is generally thought that its persistence is important for preventing loss of ozone, water and protecting planetary surfaces from energetic charged particle bombardment (e.g., Lundin et al. 2007).

Sustained periods of dynamo failure for just tens of Myr could lead to significant atmospheric loss (particularly if the stellar EUV flux is enhanced) (Lichtenegger et al. 2010). Once the mantle cools, magnetic dynamos can resume after failure as core convection reinstates (Nimmo et al. 2020). However atmospheric re-establishment of a planets H_2O and nitrogen inventory may be more difficult.

As we have discussed, Th and U are the primary contributors to radiogenic heating at late times. The abundance of these elements is commonly estimated using the surrogate element Eu. The Si content can be estimated by α element abundance being a part of the α group elements described in Section 2.1 but with the advantage of reducing the Poisson noise in the associated uncertainties of Si, Mg, Ti, and Ca through averaging.

The 1D convective model described in Nimmo et al. (2020) is adopted to predict at what $[\text{Eu}/\alpha]$ ratio a dynamo failure occurs. For an Earth-like planet, of similar composition, metallicity, and size as Earth, this model exhibits a dynamo failure of 100 Myr at $[\text{Eu}/\alpha]=0.08$ (see Figure 1). This is a conservative estimate for a critical period of dynamo collapse in which significant time has passed so that substantial atmo-

spheric loss may occur - preventing or delaying the emergence of a hospitable surface environment.

The scatter of $[\text{Eu}/\alpha]$ independent of temperature bias as a function of $[\alpha/H]$ is presented in Figure 2. Also shown is the critical value of $[\text{Eu}/\alpha]=0.08$, highlighted by the red dashed line, where an extended dynamo failure of ≥ 100 Myr occurs. Assuming that Eu and α element abundances correspond between stars and attendant planets, stars with sub-solar α -metallicity $[\alpha/H] < -0.4$ are most likely to host Earth-like planets that experience some degree of extended dynamo failure. This should be contrasted with the range of planet-forming metallicities, which is estimated to be between $-1.5 < [\alpha/H] < 0.6$ in the MW disk (e.g., Johnson & Li 2012; Ercolano & Clarke 2010; Behroozi & Peeples 2015; Boley et al. 2024). It is thus only near-solar metallicity stars that have terrestrial planet compositions supportive of a sustained magnetic dynamo.

It is important to note that this 1D model has only been configured for Earth-like planets, with the same radii, mass, and composition as the terrestrial value (e.g., Seager et al. 2007; Mordasini et al. 2012; Alibert 2014). The mass-radius scaling relation for rocky planets has recently been revised in Otegi et al. (2020) and Müller et al. (2024). Furthermore, heat production is expected to decrease at a fixed radius with increasing $[\text{Fe}/H]$ due to a larger core-to-mantle ratio O’Neill et al. (2020). It would be worth exploring in future work where a prospective “habitable metallicity zone” maps out in the radii and composition parameter space based on changing radiogenic fraction and $[\text{Fe}/H]$ (e.g., Howard et al. 2012) using a more comprehensive model including a 2D or 3D assessment of core convection.

4.2. Implications for r-Process Production

Understanding how Eu is distributed throughout the local stellar population may shed light on the source of r-process element production. The nucleosynthetic pathways and conditions for the production of r-process elements have been understood since Burbidge et al. (1957) and Cameron (1957), but the specific site(s) responsible for the modern day galactic disk enrichment of r-process elements is an area of active study (Arcones & Thielemann 2023). The primary formation sites of r-process elements are believed to be either core collapse super-

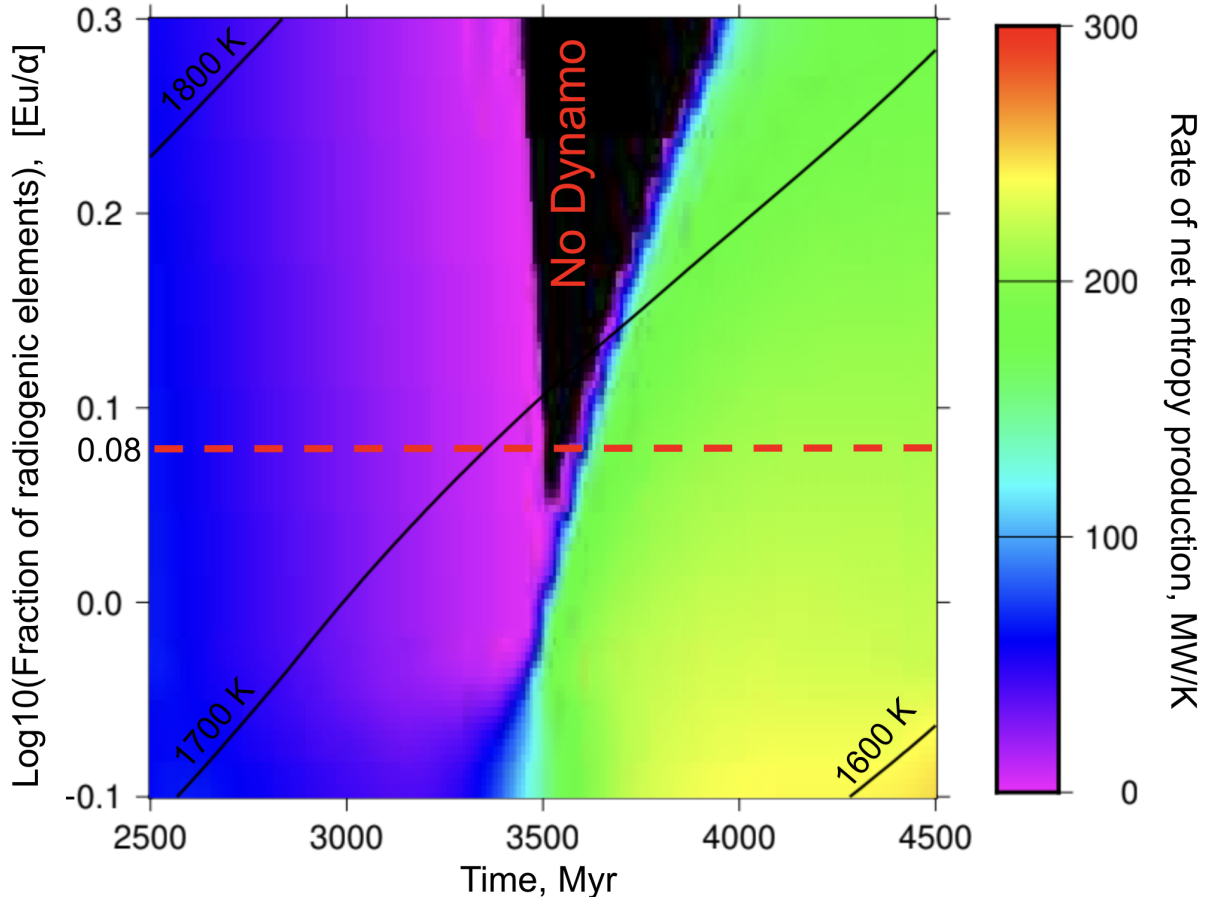


Figure 1. Illustration similar to that of Fig. 2 in Nimmo et al. (2020), demonstrating the sensitivity of core convection to changing concentrations of radiogenic elements (relative to the terrestrial amount), see Nimmo et al. (2020) for details on model parameters. Color scaled to represent net entropy production from radiogenic heating, with the black region representing negative production (no dynamo). Dashed red line represents the regime at $[\text{Eu}/\alpha]=0.08$ where a dynamo failure lasting > 100 Myr first begins. Solid black lines represent contours of constant mantle temperature.

novae (e.g., Woosley et al. 1994) or by NS-NS mergers (e.g., Lattimer & Schramm 1974). On the other hand, α elements (including O, Mg, Si, Ca, and Ti) are primarily produced in CC-SNe (Woosley & Weaver 1995). Thus by studying the distribution of r-process elements with respect to α elements the production of r-process elements can be correlated with rate of CC-SNe.

Here we focus on α , Fe, and Eu production at higher metallicities in the MW in order to derive meaningful constraints on the r-process production sites. If galactic r-process injection is dominated by CC-SNe, Eu and α will be co-produced. This predicts $[\text{Eu}/\alpha]$ to remain relatively constant with increasing $[\alpha/\text{H}]$ metallicity; in this case, the constant ratio should be representative of the IMF-weighted yield of the ejecta (Macias & Ramirez-Ruiz 2018; Kolborg et al. 2023). However, as shown in Figure 2, we find a robust anti-correlation between $[\text{Eu}/\alpha]$ and $[\alpha/\text{H}]$. The anti-correlation is consistent with a metallicity dependent r-process in CC-SNe.

Alternatively, The gravitational wave discovery of GW170817 (Abbott et al. 2017) and ensuing kilonova SSS17a/AT2017gfo (e.g., Coulter et al. 2017), provided definitive evidence of NS-NS mergers being a viable source of r-process elements but the current galactic distribution of r-process cannot be explained assuming NS-NS mergers are the only significant source of the r-process throughout cosmic time (see e.g. Siegel 2019; Chen et al. 2024, for a summary of relevant issues).

If the r-process occurs mainly in NS-NS mergers, the production of Eu is decoupled from α and Fe production (Snedden et al. 2008). The anti-correlation between $[\text{Eu}/\alpha]$ and $[\alpha/\text{H}]$ thus suggests that r-process injection from NS-NS mergers increases with time compared with α -element production. This is expected with NS-NS mergers, as they naturally experience a time delay from neutron-star pair formation to merger, which combined with the star formation history, yields a sizable increase in the number of NS-NS mergers at high metallicities

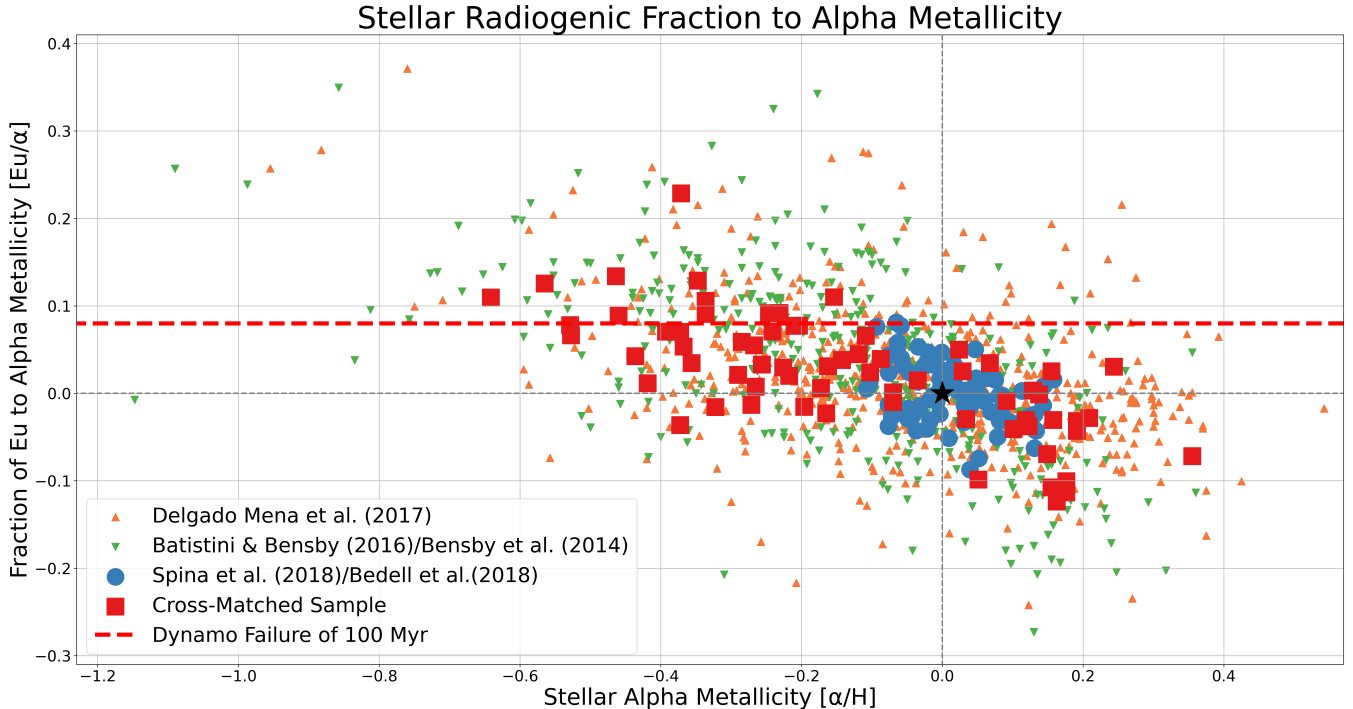


Figure 2. $[\text{Eu}/\alpha]$ independent of temperature bias as a function of $[\alpha/\text{H}]$. Small *orange* triangles represent data from DM and small *green* triangles represent data from BB. The cross matched sample of 67 stars described in Section 3.1 is shown in big *red* squares. Stars from the solar twins analysis by Spina et al. (2018), Bedell et al. (2018) are shown as big *blue* circles. A *black* star is used to represent the solar abundance value. The *red dashed* line at $[\text{Eu}/\alpha]=0.08$ represents the critical value for an extended dynamo failure given by the model from Nimmo et al. (2020).

(e.g., Shen et al. 2015). Due to the restricted metallicities used in this sample, the relative rate is subject to change at earlier periods, but for $[\alpha/\text{H}]$ between -0.7 and 0.5. The negative slope (Figure 2) suggests r-process injection by NS-NS mergers with a time delay consistent with models (e.g., Siegel 2019).

A delay-time distribution t^{-1} of NS-NS mergers predicts a flat $[\text{Eu}/\text{Fe}]$ trend with $[\text{Fe}/\text{H}]$ (e.g., Côté et al. 2019). However, this is not observed in the data (Figure 3(c)) and suggests that the delay-time distribution of NS-NS mergers differs from the t^{-1} of type Ia supernovae (e.g., Simonetti et al. 2019), which controls Fe production and is thought to be set by the merger of white dwarf binaries (e.g., Toonen et al. 2012). As such, this naturally explains the $[\text{Eu}/\text{Fe}]$ *knee* seen around $[\text{Fe}/\text{H}]=-1$ (e.g., Côté et al. 2019).

A caveat is noted when including Si, Ti and Ca in our α metallicity term. Si, Ti and Ca are fractionally produced by type Ia supernovae while Mg is exclusively produced in CC-SNe (Woodsley & Weaver 1995). A more “pure” α metallicity was tested using just $[\text{Mg}/\text{H}]$, which we found to produce similar results but with a noisier dispersion.

5. CONCLUSION

In conclusion, we have identified metallicity ($[\alpha/\text{H}]$) and temperature (T_{eff}) as relevant systematic biases inflating the observed scatter of $[\text{Eu}/\text{H}]$. We measured the intrinsic star-to-star scatter of detrended $[\text{Eu}/\text{H}]$ as a function of $[\alpha/\text{H}]$ and T_{eff} to be 0.025 dex, consistent with a chemically well-mixed stellar neighborhood.

Th and U are the primary isotopes responsible for radiogenic mantle heating in rocky planets that are several Gyr old. Assuming that planetary compositions reflect their stellar host’s atmospheric abundances, we use Eu as a proxy for Th and U and employ a 1D thermal evolutionary model from Nimmo et al. (2020). Modeling suggests a significant dynamo failure lasting at least ≥ 100 Myr beginning at a $[\text{Eu}/\alpha] = 0.08$ dex. Stars hosting earth-composition and size planets at or above this critical value are likely to have experienced a dynamo collapse for an extended period of time, leaving the surface vulnerable to atmospheric stripping and charged particle bombardment - conditions immediately challenging for a hospitable biosphere. Although the dynamo may reinstate after sufficient mantle cooling, it is unclear if reestablishment of an atmosphere is possible. The anticorrelation between $[\text{Eu}/\alpha]$ and $[\alpha/\text{H}]$ would imply that only near-solar α -metallicity stars have $[\text{Eu}/\alpha]$ content

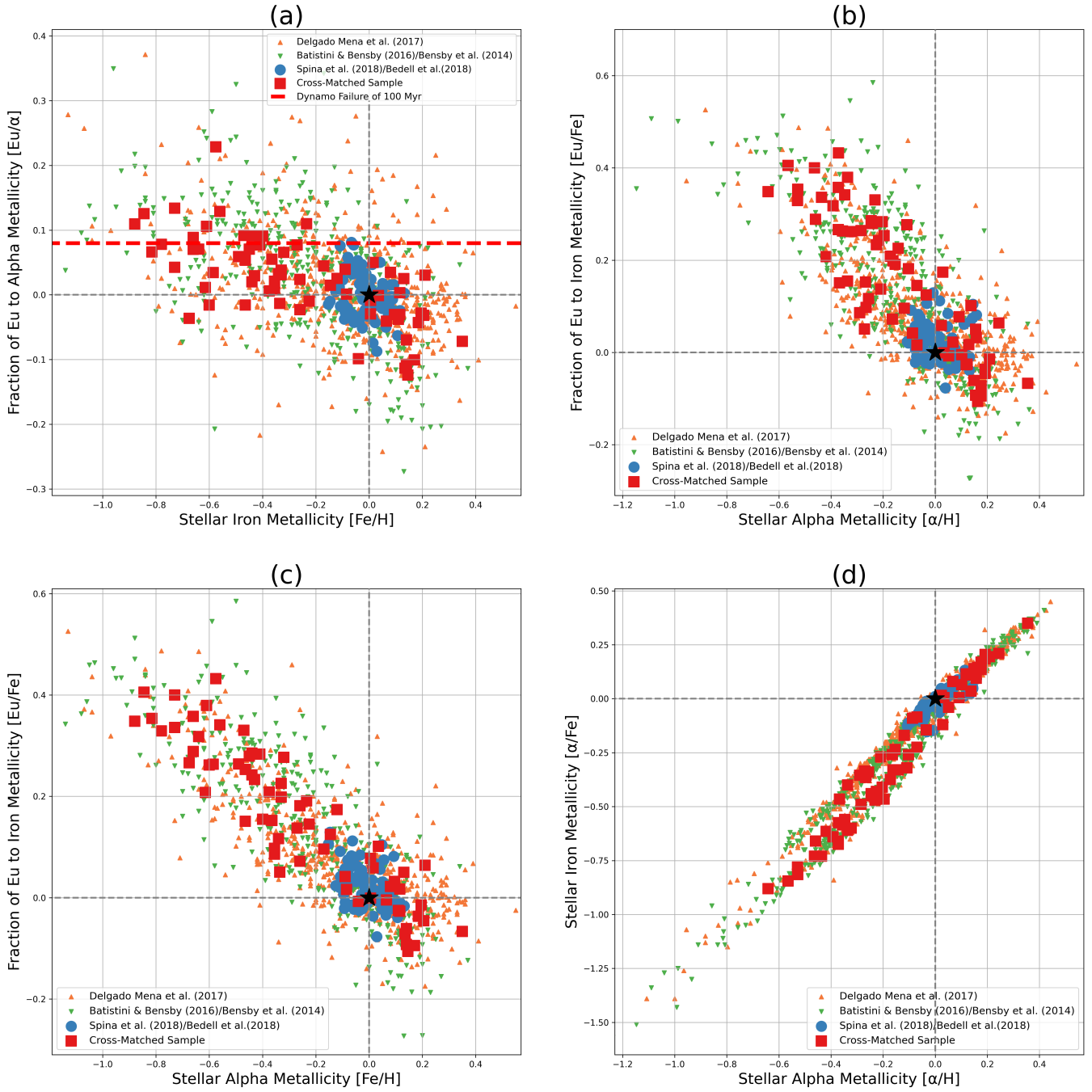


Figure 3. Constraints on r-process production sites derived from stellar abundances. (a) Top right panel shows $[Eu/\alpha]$ independent of the temperature bias as a function of $[\alpha/H]$. (b) Top left panel shows $[Eu/Fe]$ independent of the temperature bias as a function of $[\alpha/H]$. (c) Bottom left shows $[Eu/\alpha]$ independent of the temperature bias as a function of $[Fe/H]$. (d) Bottom right panel shows $[\alpha/H]$ to $[Fe/H]$. The same legend is used as Figure 2

supportive of persistent dynamos on attendant terrestrial planets.

Lastly, this anti-correlation lends clues as to the primary r-process injection site in the MW. Assuming r-process production is dominated by CC-SNe, the observed anti-correlation may be explained by a metallicity dependent r-process. Alternatively, assuming that r-process injection is dominated by NS-NS mergers, the slope of the anti-correlation would give the relative production rate between r-process in NS-NS mergers and α elements in core collapse supernovae, which is naturally explained by the time-delay distribution expected for NS-NS mergers. Furthermore, the anti-correlation between [Eu/Fe] and [Fe/H], also implies that the delay-time distribution of NS-NS mergers, if responsible for the bulk of r-process production, differs from that of type Ia supernovae.

6. ACKNOWLEDGMENTS

This work makes use of the Astrophysics Data System, funded by NASA under Cooperative Agreement 80NSSC21M00561, the SIMBAD database operated at CDS, Strasbourg, France (Wenger et al. 2000), the VizieR catalogue access tool, CDS, Strasbourg, France (Ochsenbein 1996), and IRAF, distributed by the National Optical Astronomy Observatories (Tody 1986). The original description of the VizieR service was published in Ochsenbein et al. (2000).

We thank S. Faber for fruitful discussions and guidance. ER-R supported in part by the Heising-Simons Foundation and the National Science Foundation (AST-2307710, AST-2206243, AST-1911206, and AST-1852393). EMC supported in part by the University of California, Santa Cruz, Undergraduate Research in Science & Technology Award.

7. APPENDIX

7.1. Solar Twins Analysis

The determined dispersion in detrended [Eu/H] of ± 0.025 dex is further corroborated by data from a solar twins analysis by Spina et al. (2018) and Bedell et al. (2018). This sample of 79 stars uses near solar parameters with temperature within ± 100 K in T_{eff} , [Fe/H] within ± 0.1 dex and surface gravity within ± 0.1 dex in $\text{Log } g$ of the solar value. These restricted parameters combined with high S/N and high resolution contribute to exceptionally low quoted uncertainties on abundance measurements.

We repeat the same simultaneous contour-fit methodology described in Section 2.3 to create an expression for detrended [Eu/H] as a function of metallicity and temperature under the solar twins sample. We fit these

two terms to [Eu/H] simultaneously in a linear surface-fit polynomial with an intercept of -1.534 ± 0.112 dex, metallicity slope of 0.789 ± 0.018 , and temperature slope of $2.7434 \times 10^{-4} \pm 1.944 \times 10^{-5}$ dex, with a reduced $\chi^2=10.22$ and standard deviation of 0.031. The reduced χ^2 is notably high, consequence of exceptionally low quoted uncertainties in elemental abundance measurements.

In our earlier analysis we were able to cross match detrended [Eu/H] measurements in an effort to further reduce the dispersion. However, the sample from Spina et al. (2018) and Bedell et al. (2018) shares no stars in common with either DM or BB. Instead, tweaking the formalism described in Section 3.2 we can reduce the dispersion in detrended [Eu/H] further. Due to the exceptionally low uncertainty in [Eu/H], we claim that the error on [Eu/H] is solely the uncertainty contributed by Poisson noise. In this way, the dispersion of detrended [Eu/H] is given as:

$$\sigma_{\text{detrended[Eu/H]}}^2 = \sigma_{\text{Poisson}}^2 + \sigma_{\text{intrinsic}}^2 \quad (4)$$

Re-arranging this equation and assuming the error on [Eu/H] is entirely the Poisson noise $\sigma_{\text{Poisson}} = 0.012$ dex (using the mean of the error on [Eu/H]), the intrinsic dispersion is determined as $\sigma_{\text{intrinsic}} = 0.029$ dex.

Without a secondary analysis to compare against, we cannot reduce the dispersion any further. The intrinsic dispersion determined here is supportive of the dispersion calculated in Section 3.1. This suggests we are indeed approaching a star-to-star dispersion reflective of the actual stellar chemical environment in the local stellar neighborhood.

7.2. Potential outliers

Within the samples used, a handful of outliers in [Eu/H] abundance have been identified. We consider an outlier as any star whose detrended [Eu/H] value is greater than 3 standard deviations (SD) from the mean. These stars are worth particular attention for two reasons, their unusual [Eu/H] abundance contributes to the inflation of the intrinsic dispersion significantly and secondly these stars may have unique chemical-evolutionary histories worth investigating.

Under the cross-matched sample as described in Section 3.1 there is one outlier. The cross-matched sample has a significantly smaller SD than in the full samples due to reduced uncertainties from averaging, stars that appear as outliers in the full samples do not reappear in the cross matched sample.

In the sample from DM, containing 570 stars with [Eu/H] abundance measurements, the standard deviation was found to be 0.071 (methodology described in

Designation	Detrended [Eu/H] (dex)	Standard Deviations	Sample
HD85512	0.244	3.459	Delgado Mena
HD218511	0.259	3.659	Delgado Mena
BD+062932	0.253	3.579	Delgado Mena
HD73267	-0.223	-3.153	Delgado Mena
HD190954	-0.249	-3.522	Delgado Mena
HD167677	0.258	3.654	Delgado Mena
HD209458	0.218	3.079	Delgado Mena
HD148156	0.255	3.612	Delgado Mena
HD205591	0.229	3.237	Delgado Mena
HIP73385	0.273	3.375	Battistini & Bensby
HIP81041	-0.279	-3.447	Battistini & Bensby
HIP81461	0.270	3.329	Battistini & Bensby
HIP95106	0.301	3.722	Battistini & Bensby
HD11397	0.156	3.343	Cross-matched Sample

Table 2. Shown are the 9 stars from DM and 4 stars from BB with detrended [Eu/H] abundance >3 SD. Stars only appearing in a single sample use detrended [Eu/H] formulae and SD described in Section 2.3. Stars in the cross-matched sample use an averaged detrended [Eu/H] formulae and SD described in Section 3.1. The last bold entry represents the single star from the cross-matched sample to be > 3 SD. No stars were determined as outliers from the solar twins analysis by Spina et al. (2018) and Bedell et al. (2018).

2.3). Under this standard deviation, 9 stars are measured with detrended [Eu/H] greater than 3 SD from the mean. These stars are listed in Table 2. Assuming the sample follows a normal Gaussian distribution, we would only expect 1-2 stars above 3 SD in a sample size of 577, this suggests the existence of at most 7 statistical outliers in detrended [Eu/H].

Using a similar analysis, in the sample from BB, containing 377 stars with valid [Eu/H] and $[\alpha/\text{H}]$ abundance measurements, the standard deviation is found to be 0.081. Under this standard deviation, 3 stars are measured with detrended [Eu/H] of greater than 3 SD. These stars are listed in Table 2. Following a normal Gaussian distribution, we only expect 1 star above 3 SD in a sample size of 377, this suggests the existence of at most 2 statistical outliers in detrended [Eu/H].

In the cross-matched sample, HD11397 has a detrended [Eu/H] abundance of 0.150 dex pushing it out to 3.192 SDs from the mean trend; see Table 2 in bold. This star is likely to be real outlier as its unusual detrended [Eu/H] measurement is corroborated by both data sets.

No outliers were found in the sample from Spina et al. (2018) and Bedell et al. (2018). This may be owed to the small sample size and/or the exceptionally small quoted uncertainties.

These stars' odd compositions may be a result of a particularly r-process rich birth cloud or another heavy element doping mechanism such as a binary-supernova pair. Further analysis is needed to determine the unique properties of the stars listed.

REFERENCES

- Abbott, B. P., Abbott, R., Abbott, T. D., et al. 2017, *PhRvL*, 119, 161101, doi: [10.1103/PhysRevLett.119.161101](https://doi.org/10.1103/PhysRevLett.119.161101)
- Alibert, Y. 2014, *A&A*, 561, A41, doi: [10.1051/0004-6361/201322293](https://doi.org/10.1051/0004-6361/201322293)
- Arcones, A., & Thielemann, F.-K. 2023, *A&A Rv*, 31, 1, doi: [10.1007/s00159-022-00146-x](https://doi.org/10.1007/s00159-022-00146-x)
- Arnould, M., Goriely, S., & Takahashi, K. 2007, *PhR*, 450, 97, doi: [10.1016/j.physrep.2007.06.002](https://doi.org/10.1016/j.physrep.2007.06.002)
- Battistini, C., & Bensby, T. 2016, *A&A*, 586, A49, doi: [10.1051/0004-6361/201527385](https://doi.org/10.1051/0004-6361/201527385)
- Bedell, M., Bean, J. L., Meléndez, J., et al. 2018, *ApJ*, 865, 68, doi: [10.3847/1538-4357/aad908](https://doi.org/10.3847/1538-4357/aad908)
- Behroozi, P., & Peebles, M. S. 2015, *MNRAS*, 454, 1811, doi: [10.1093/mnras/stv1817](https://doi.org/10.1093/mnras/stv1817)
- Bensby, T., Feltzing, S., & Oey, M. S. 2014, *A&A*, 562, A71, doi: [10.1051/0004-6361/201322631](https://doi.org/10.1051/0004-6361/201322631)
- Boley, K. M., Christiansen, J. L., Zink, J., et al. 2024, *AJ*, 168, 128, doi: [10.3847/1538-3881/ad6570](https://doi.org/10.3847/1538-3881/ad6570)
- Bono, R. K., Tarduno, J. A., Nimmo, F., & Cottrell, R. D. 2019, *Nature Geoscience*, 12, 143

- Botelho, R. B., Milone, A. d. C., Meléndez, J., et al. 2019, *MNRAS*, 482, 1690, doi: [10.1093/mnras/sty2791](https://doi.org/10.1093/mnras/sty2791)
- Boujibar, A., Driscoll, P., & Fei, Y. 2020, *Journal of Geophysical Research (Planets)*, 125, e06124, doi: [10.1029/2019JE006124](https://doi.org/10.1029/2019JE006124)
- Burbidge, E. M., Burbidge, G. R., Fowler, W. A., & Hoyle, F. 1957, *Reviews of Modern Physics*, 29, 547, doi: [10.1103/RevModPhys.29.547](https://doi.org/10.1103/RevModPhys.29.547)
- Cameron, A. G. W. 1957, *PASP*, 69, 201, doi: [10.1086/127051](https://doi.org/10.1086/127051)
- Cescutti, G., François, P., & Matteucci, F. 2005, in *IAU Symposium*, Vol. 228, *From Lithium to Uranium: Elemental Tracers of Early Cosmic Evolution*, ed. V. Hill, P. François, & F. Primas, 445–450, doi: [10.1017/S1743921305006198](https://doi.org/10.1017/S1743921305006198)
- Chen, M.-H., Li, L.-X., Chen, Q.-H., Hu, R.-C., & Liang, E.-W. 2024, *MNRAS*, 529, 1154, doi: [10.1093/mnras/stae475](https://doi.org/10.1093/mnras/stae475)
- Côté, B., Eichler, M., Arcones, A., et al. 2019, *ApJ*, 875, 106, doi: [10.3847/1538-4357/ab10db](https://doi.org/10.3847/1538-4357/ab10db)
- Coulter, D. A., Foley, R. J., Kilpatrick, C. D., et al. 2017, *Science*, 358, 1556, doi: [10.1126/science.aap9811](https://doi.org/10.1126/science.aap9811)
- Cowan, J. J., & Thielemann, F.-K. 2004, *Physics Today*, 57, 10.47, doi: [10.1063/1.1825268](https://doi.org/10.1063/1.1825268)
- Delgado Mena, E., Tsantaki, M., Adibekyan, V. Z., et al. 2017, *A&A*, 606, A94, doi: [10.1051/0004-6361/201730535](https://doi.org/10.1051/0004-6361/201730535)
- Ercolano, B., & Clarke, C. J. 2010, *MNRAS*, 402, 2735, doi: [10.1111/j.1365-2966.2009.16094.x](https://doi.org/10.1111/j.1365-2966.2009.16094.x)
- Foley, B. J., & Smye, A. J. 2018, *Astrobiology*, 18, 873, doi: [10.1089/ast.2017.1695](https://doi.org/10.1089/ast.2017.1695)
- Frank, E. A., Meyer, B. S., & Mojszsis, S. J. 2014, *Icarus*, 243, 274, doi: [10.1016/j.icarus.2014.08.031](https://doi.org/10.1016/j.icarus.2014.08.031)
- Gunell, H., Maggiolo, R., Nilsson, H., et al. 2018, *A&A*, 614, L3, doi: [10.1051/0004-6361/201832934](https://doi.org/10.1051/0004-6361/201832934)
- Holmbeck, E. M., Sprouse, T. M., & Mumpower, M. R. 2023, *European Physical Journal A*, 59, 28, doi: [10.1140/epja/s10050-023-00927-7](https://doi.org/10.1140/epja/s10050-023-00927-7)
- Howard, A. W., Marcy, G. W., Bryson, S. T., et al. 2012, *ApJS*, 201, 15, doi: [10.1088/0067-0049/201/2/15](https://doi.org/10.1088/0067-0049/201/2/15)
- Jellinek, A. M., & Jackson, M. G. 2015, *Nature Geoscience*, 8, 587, doi: [10.1038/ngeo2488](https://doi.org/10.1038/ngeo2488)
- Ji, A. P., Frebel, A., Chiti, A., & Simon, J. D. 2016, *Nature*, 531, 610, doi: [10.1038/nature17425](https://doi.org/10.1038/nature17425)
- Johnson, J. L., & Li, H. 2012, *ApJ*, 751, 81, doi: [10.1088/0004-637X/751/2/81](https://doi.org/10.1088/0004-637X/751/2/81)
- Kasen, D., Metzger, B., Barnes, J., Quataert, E., & Ramirez-Ruiz, E. 2017, *Nature*, 551, 80, doi: [10.1038/nature24453](https://doi.org/10.1038/nature24453)
- Kolborg, A. N., Ramirez-Ruiz, E., Martizzi, D., Macias, P., & Soares-Furtado, M. 2023, *ApJ*, 949, 100, doi: [10.3847/1538-4357/acca80](https://doi.org/10.3847/1538-4357/acca80)
- Labrosse, S. 2014, *Comptes Rendus Geoscience*, 346, 119, doi: [10.1016/j.crte.2014.04.005](https://doi.org/10.1016/j.crte.2014.04.005)
- . 2015, *Physics of the Earth and Planetary Interiors*, 247, 36, doi: [10.1016/j.pepi.2015.02.002](https://doi.org/10.1016/j.pepi.2015.02.002)
- Lattimer, J. M., & Schramm, D. N. 1974, *ApJL*, 192, L145, doi: [10.1086/181612](https://doi.org/10.1086/181612)
- Lichtenegger, H. I. M., Lammer, H., Grießmeier, J. M., et al. 2010, *Icarus*, 210, 1, doi: [10.1016/j.icarus.2010.06.042](https://doi.org/10.1016/j.icarus.2010.06.042)
- Lundin, R., Lammer, H., & Ribas, I. 2007, *SSRv*, 129, 245, doi: [10.1007/s11214-007-9176-4](https://doi.org/10.1007/s11214-007-9176-4)
- Macias, P., & Ramirez-Ruiz, E. 2018, *ApJ*, 860, 89, doi: [10.3847/1538-4357/aac3e0](https://doi.org/10.3847/1538-4357/aac3e0)
- . 2019, *ApJL*, 877, L24, doi: [10.3847/2041-8213/ab2049](https://doi.org/10.3847/2041-8213/ab2049)
- Mello, F. d. S., & Friaça, A. C. S. 2023, *International Journal of Astrobiology*, 22, 272, doi: [10.1017/S1473550423000083](https://doi.org/10.1017/S1473550423000083)
- Mordasini, C., Alibert, Y., Georgy, C., et al. 2012, *A&A*, 547, A112, doi: [10.1051/0004-6361/201118464](https://doi.org/10.1051/0004-6361/201118464)
- Mösta, P., Roberts, L. F., Halevi, G., et al. 2018, *ApJ*, 864, 171, doi: [10.3847/1538-4357/aad6ec](https://doi.org/10.3847/1538-4357/aad6ec)
- Müller, S., Baron, J., Helled, R., Bouchy, F., & Parc, L. 2024, *A&A*, 686, A296, doi: [10.1051/0004-6361/202348690](https://doi.org/10.1051/0004-6361/202348690)
- Naiman, J. P., Pillepich, A., Springel, V., et al. 2018, *MNRAS*, 477, 1206, doi: [10.1093/mnras/sty618](https://doi.org/10.1093/mnras/sty618)
- Nichols, C. I. O., Weiss, B. P., Eyster, A., et al. 2024, *Journal of Geophysical Research (Solid Earth)*, 129, e2023JB027706, doi: [10.1029/2023JB02770610.31223/x5sx0v](https://doi.org/10.1029/2023JB02770610.31223/x5sx0v)
- Nimmo, F., Primack, J., Faber, S. M., Ramirez-Ruiz, E., & Safarzadeh, M. 2020, *The Astrophysical Journal Letters*, 903, L37, doi: [10.3847/2041-8213/abc251](https://doi.org/10.3847/2041-8213/abc251)
- Ochsenbein, F. 1996, *The VizieR database of astronomical catalogues*, CDS, Centre de Donn  es astronomiques de Strasbourg, doi: [10.26093/CDS/VIZIER](https://doi.org/10.26093/CDS/VIZIER)
- Ochsenbein, F., Bauer, P., & Marcout, J. 2000, *A&AS*, 143, 23, doi: [10.1051/aas:2000169](https://doi.org/10.1051/aas:2000169)
- O’Neill, C., Lowman, J., & Wasiliev, J. 2020, *Icarus*, 352, 114025, doi: [10.1016/j.icarus.2020.114025](https://doi.org/10.1016/j.icarus.2020.114025)
- Otegi, J. F., Bouchy, F., & Helled, R. 2020, *A&A*, 634, A43, doi: [10.1051/0004-6361/201936482](https://doi.org/10.1051/0004-6361/201936482)
- Quick, L. C., Roberge, A., Mlinar, A. B., & Hedman, M. M. 2020, *PASP*, 132, 084402, doi: [10.1088/1538-3873/ab9504](https://doi.org/10.1088/1538-3873/ab9504)
- Seager, S., Kuchner, M., Hier-Majumder, C. A., & Militzer, B. 2007, *ApJ*, 669, 1279, doi: [10.1086/521346](https://doi.org/10.1086/521346)

- Shen, S., Cooke, R. J., Ramirez-Ruiz, E., et al. 2015, *ApJ*, 807, 115, doi: [10.1088/0004-637X/807/2/115](https://doi.org/10.1088/0004-637X/807/2/115)
- Siegel, D. M. 2019, *European Physical Journal A*, 55, 203, doi: [10.1140/epja/i2019-12888-9](https://doi.org/10.1140/epja/i2019-12888-9)
- Siegel, D. M., Barnes, J., & Metzger, B. D. 2019, *Nature*, 569, 241, doi: [10.1038/s41586-019-1136-0](https://doi.org/10.1038/s41586-019-1136-0)
- Simonetti, P., Matteucci, F., Greggio, L., & Cescutti, G. 2019, *MNRAS*, 486, 2896, doi: [10.1093/mnras/stz991](https://doi.org/10.1093/mnras/stz991)
- Snedden, C., Cowan, J. J., & Gallino, R. 2008, *ARA&A*, 46, 241, doi: [10.1146/annurev.astro.46.060407.145207](https://doi.org/10.1146/annurev.astro.46.060407.145207)
- Spina, L., Meléndez, J., Karakas, A. I., et al. 2018, *MNRAS*, 474, 2580, doi: [10.1093/mnras/stx2938](https://doi.org/10.1093/mnras/stx2938)
- Tody, D. 1986, in *Society of Photo-Optical Instrumentation Engineers (SPIE) Conference Series*, Vol. 627, *Instrumentation in astronomy VI*, ed. D. L. Crawford, 733, doi: [10.1117/12.968154](https://doi.org/10.1117/12.968154)
- Toonen, S., Nelemans, G., & Portegies Zwart, S. 2012, *A&A*, 546, A70, doi: [10.1051/0004-6361/201218966](https://doi.org/10.1051/0004-6361/201218966)
- Unterborn, C. T., Johnson, J. A., & Panero, W. R. 2015, *ApJ*, 806, 139, doi: [10.1088/0004-637X/806/1/139](https://doi.org/10.1088/0004-637X/806/1/139)
- Wang, H. S., Morel, T., Quanz, S. P., & Mojzsis, S. J. 2020, *A&A*, 644, A19, doi: [10.1051/0004-6361/202038386](https://doi.org/10.1051/0004-6361/202038386)
- Wenger, M., Ochsenbein, F., Egret, D., et al. 2000, *A&AS*, 143, 9, doi: [10.1051/aas:2000332](https://doi.org/10.1051/aas:2000332)
- Wienbruch, U., & Spohn, T. 1995, *Planet. Space Sci.*, 43, 1045, doi: [10.1016/0032-0633\(95\)00039-8](https://doi.org/10.1016/0032-0633(95)00039-8)
- Woolley, S. E., & Weaver, T. A. 1995, *ApJS*, 101, 181, doi: [10.1086/192237](https://doi.org/10.1086/192237)
- Woolley, S. E., Wilson, J. R., Mathews, G. J., Hoffman, R. D., & Meyer, B. S. 1994, *ApJ*, 433, 229, doi: [10.1086/174638](https://doi.org/10.1086/174638)
- Zhang, J., & Rogers, L. A. 2022, *ApJ*, 938, 131, doi: [10.3847/1538-4357/ac8e65](https://doi.org/10.3847/1538-4357/ac8e65)